PAPER

Ultrafast photoinduced dynamics of halogenated cyclopentadienes: observation of geminate charge-transfer complexes in solution†

T. J. A. Wolf,*[a] O. Schalk,[bcd] R. Radloff,[a] G. Wu,[be] P. Lang,[c] A. Stolow[b] and A.-N. Unterreiner*[a]

The photoinduced dynamics of the fully halogenated cyclopentadienes C_5Cl_6 and C_5Br_6 have been investigated in solution and gas phase by femtosecond time-resolved spectroscopy. Both in solution and in gas phase, homolytic dissociation into a halogen radical and a C_5X_5 (X = Cl, Br) radical was observed. In liquid phase, solvent-dependent formation of charge transfer complexes between geminate radicals was observed for the first time. These complexes were found to be surprisingly stable and offered the opportunity to follow the dynamics of specific radical pairs. In the case of C_5Cl_6 in trichloroethanol, a reaction of the chlorine radical with molecules from the solvent cage was observed.

1 Introduction

The kinetics and behavior of photo-generated radicals in solution are important issues in many fields of research, including atmospheric chemistry in clouds[1] and photopolymerization.[2] In particular, the behavior of halogen radicals originating from photodegradation of environmental pollutants in solution is a significant field of investigation.[3,4] Bromine and chlorine radicals form charge-transfer (CT) complexes with many solvents and, therefore, exhibit characteristic absorption bands in the visible and the UV.[5–14] These complexes are known to be very short-lived and to influence the reactivity of the radicals towards H abstraction. The charge-transfer absorption band can potentially act as a highly sensitive tool for investigating the formation and destruction of an individual complex. Therefore, we looked for a system which after photoinduced bond fission forms a CT complex itself.

[a] Institut für Physikalische Chemie and Center for Functional Nanostructures (CFN), Karlsruhe Institute of Technology (KIT), Fritz-Haber-Weg 2, 76131 Karlsruhe, Germany. E-mail: thomas.wolf@kit.edu, andreas.unterreiner@kit.edu; Fax: +49 721 608 46524; Tel: +49 721 608 48022
[b] National Research Council, 100 Sussex Drive, Ottawa, K1A 0R6, Canada
[c] Lehrstuhl für BioMolekulare Optik, Ludwig-Maximilians-Universität München, Oettingenstr. 67, 80538 München, Germany
[d] Stockholm University, AlbaNova University Center, SE-10691, Stockholm, Sweden
[e] State Key Laboratory of Molecular Reaction Dynamics, Dalian Institute of Chemical Physics, Chinese Academy of Sciences, Dalian, Liaoning 116023, P. R. China
† Electronic supplementary information (ESI) available. See DOI: 10.1039/c3cp44295k

A suitable geminate CT complex has to be reasonably stabilized against geminate recombination or electron transfer, which can lead to ion pairs instead of radical pairs. Such an electron transfer, following homolytic bond dissociation, was recently shown to take place within 10 ps in the photogeneration of the benzhydryl cation in solution.[15,16] Additionally, geminate recombination was observed as a side reaction.

We were inspired by studies of Graf and Günthard, who observed photoinduced radical formation from fully chlorinated (C_5Cl_6) and brominated cyclopentadienes (C_5Br_6) *via* homolytic fission of a carbon–halogen bond at the sp^3 position of the five-membered ring after irradiation with a xenon lamp.[17–19] Using EPR spectroscopy in solution, the resulting cyclopentadienyl radicals were observed to be planar and highly symmetrical (D_{5h}). When irradiating solutions of C_5Br_6 in a frozen solvent at liquid nitrogen temperatures, formation of a broad absorption band peaking at 480 nm was observed. Upon thawing the sample, the absorption disappeared. The absorption band was, therefore, assigned to geminate formation of a $C_5Br_5\cdots Br$ CT complex in the frozen solvent cage, and its destruction due to diffusion of the radicals upon thawing of the frozen solvent cage. However, in C_5Cl_6 no additional CT absorption band could be observed.

In comparison to *e.g.* benzhydryl chloride, where the photogenerated benzhydryl radical experiences a considerable stabilization *via* an electron transfer to the chlorine radical, and therewith oxidation to an aromatic electron configuration,[15,16] the cyclopentadienyl radical can become aromatic only by reduction, *i.e.* acceptance of an electron. Since reduction by a halogen

radical is rather unlikely, at least this geminate quenching channel can be ruled out.

The excited states of cyclopentadiene (C_5H_6) were the subject of many experimental and theoretical investigations.[20–30] The role of a low lying, spectroscopically dark excited singlet state with partially doubly excited character is a subject of current discussion.[30] As it is known to undergo radiationless relaxation after photoexcitation within several tens of fs, the photolytic bond fission observed in the halogenated analogues can be expected to take place on a similar time scale.[31]

Therefore, C_5Cl_6 and C_5Br_6 are comparatively investigated by femtosecond transient absorption spectroscopy in the solvents cyclohexane, isopropanol, chloroform, and trichloroethanol, which are expected to exhibit a largely differing reactivity towards H abstraction by chlorine radicals.[13]

In many cases, it is difficult to disentangle excited state dynamics of the originally excited molecule from vibrational cooling in the ground state, additional ground state dynamics of photoproducts and their interaction with the solvent by solely considering photoinduced dynamics in solution. Hence, C_5Cl_6 and C_5Br_6 are also investigated by time-resolved photoelectron spectroscopy in the gas phase. Due to the missing solvent environment only purely excited state dynamics of the two compounds are expected to be observable in this case.

2 Experimental

2.1 Sample preparation

C_5Cl_6 (purity: 99%) was purchased from Dr Ehrenstorfer[39] and used without further purification. The synthesis of C_5Br_6 was adapted from the literature.[40] A ^{13}C-NMR spectrum is depicted in Fig. S1 in the ESI.† The purity is estimated to be >95%. Solvents were purchased from Sigma Aldrich and Carl Roth.

Steady state absorption spectra were obtained using a Varian Cary 500 spectrometer in fused silica cuvettes with an optical pathlength of 1 mm.

2.2 Femtosecond transient absorption spectroscopy in solution

The details of the experimental setup are described elsewhere.[41] Briefly, pump pulses at central wavelengths (λ_p) of 323 nm (C_5Cl_6) and 350 nm (C_5Br_6) were produced using an UV-NOPA (ultraviolet noncollinear optical parametric amplifier).[42,43] Probe pulses at wavelengths between 500 nm and 1050 nm at a polarisation plane at magic angle relative to the pump pulses were produced using a second NOPA. The pump intensity was kept below 4×10^8 W cm^{-2} to ensure that only small changes in optical density occur. The time resolution was measured by cross-correlation in the dyes BBQ (λ_p = 323 nm) and stilbene 3 (λ_p = 350 nm) to be always below 100 fs. Samples were measured at 20 °C in a flow cell system including a fused silica cuvette with an optical pathlength of 1 mm. Rapid photodegradation of all samples was observed. To reduce effects of group velocity mismatch, the optical density of the solutions was kept above 3 at the respective excitation wavelengths, which resulted in a reduced effective optical pathlength for
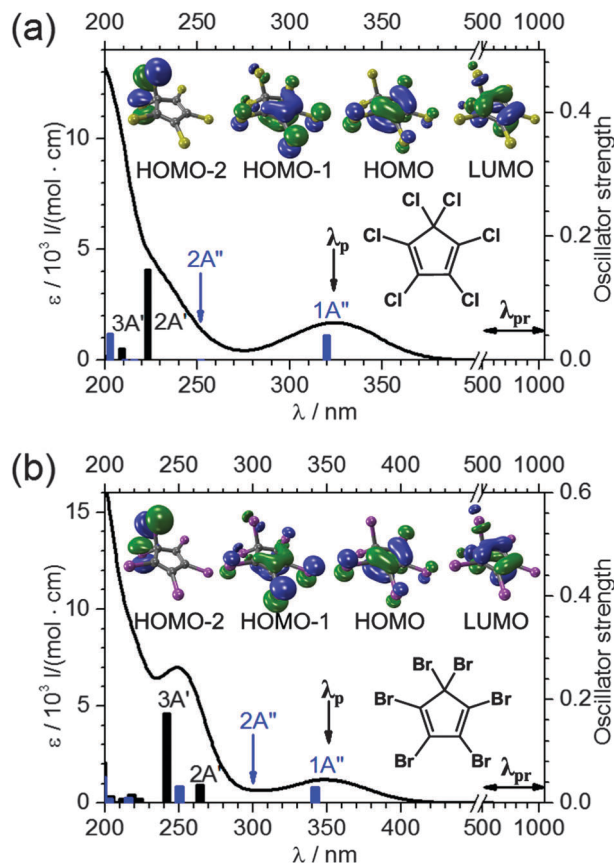

Fig. 1 Extinction coefficients of (a) C_5Cl_6 and (b) C_5Br_6 in cyclohexane solution together with singlet transitions calculated with CC2/aug-cc-pVDZ. Transitions to A′ states are colored in black, excitations to A″ states in blue. Selected transitions are labeled. Furthermore, visualizations of the MOs, which are most relevant for the selected transitions, are inserted. Moreover, λ_p and the λ_{pr} range of the transient absorption experiments are marked.

the experiments. The concentrations were thus in the range of 2.5×10^{-2} mol l^{-1}, depending on the extinction coefficients of C_5Cl_6 and C_5Br_6 at the respective λ_p (see Fig. 1).

2.3 Time resolved photoelectron spectroscopy (TRPES)

For time resolved experiments in the gas phase a photoelectron spectrometer was employed, consisting of a femtosecond laser system and a magnetic bottle time of flight spectrometer in combination with a supersonic molecular beam. The experimental setup is described in detail elsewhere.[44] Briefly, pump pulses at λ_p = 315 nm were generated by frequency quadrupling of the output of an optical parametric amplifier. Energies were 1.5 μJ (at λ_{pr} = 267 nm) and 1.6 μJ (at λ_{pr} = 400 nm). For the probe wavelengths of λ_{pr} = 266 nm (3.2 μJ) and 400 nm (19 μJ) a part of the laser output at 800 nm was frequency tripled or frequency doubled, respectively. The relative polarization of pump and probe pulses was rotated to magic angle. The pulses were collinearly focused into the interaction chamber of the photoelectron spectrometer. Photoelectron energies were calibrated by using the known photoelectron spectrum[45] of NO and the cross correlation of pump and probe pulses was measured to be 140 fs by analyzing a nonresonant 3-photon ([2,1′] or [1,2′])

ionization peak of NO. In the interaction chamber a supersonic molecular beam generated by a 1 kHz Even–Lavie valve with a 200 μm diameter conical nozzle perpendicularly crossed the optical beam path. Helium was used as a carrier gas with a backing pressure of 3.8 bar. C_5Cl_6 was introduced into the body of the valve as a liquid, soaked into a filter paper. C_5Br_6 was introduced as a solid with additional filter paper. C_5Cl_6 was slightly heated to 40 °C, C_5Br_6 to 80 °C, to enhance the vapor pressure. To prevent condensation of the sample in the nozzle of the valve the frontplate of the valve was separately heated. Based on prior experience, the rotational and vibrational temperatures within the molecular beam can be assumed to exhibit values of 10–20 K and 100 K, respectively.

2.4 Theoretical methods

Geometry optimizations, ground state, excitation energies and ionization potentials were calculated employing the TURBO-MOLE V-6.3 program package.[46] Geometry optimizations in the electronic ground state were performed with BP86/def2-SV(P).[47–51] Ground state energies, first-order properties, and excitation energies were calculated with CC2/aug-cc-pVDZ[52–55] as well as TDDFT/B3LYP/aug-cc-pVDZ.[55–58] Ionization potentials were calculated with CCSD/def2-TZVP.[52–54,59] For CASSCF calculations, the COLUMBUS V5.9 (ref. 60–63) program package was employed.

3 Results

3.1 Steady state spectroscopy

The absorption spectra of C_5Cl_6 and C_5Br_6 in cyclohexane solution are depicted in Fig. 1 (a) and (b) together with calculated excitation spectra (CC2/aug-cc-pVDZ).

The ground state minimum geometries of C_5Cl_6 and C_5Br_6 both exhibit C_{2v} symmetry. However, for a nomenclature of the excited states, which is consistent with the photoproducts, all electronic states are labeled according to the C_s symmetry group. Transitions to selected excited states, which are important for the later discussion, are explicitly marked in Fig. 1. The MOs, which are most relevant for these transitions are additionally depicted. As could be expected from the employed method, excitation energies are slightly overestimated by the calculation.

The first absorption band of C_5Cl_6 at λ = 323 nm can be assigned to a $\pi\pi^*$ LUMO ← HOMO transition (see Fig. 1 (a)) from the closed shell 1A′ ground state to the lowest state with A″ symmetry (1A″), which is in good agreement with the known excited states of C_5H_6.[21,23,25,27]

The second excited state (labeled as 2A″ in Fig. 1 (a)) shows strong Rydberg character and is calculated to exhibit zero oscillator strength. Accordingly, it is not found in the experimental absorption spectrum. The 2A′ state has mainly the character of a $\pi\pi^*$ LUMO ← HOMO−1 transition. This state is probably the analogue to the multiconfigurational $2A_1$ state with additional doubly excited character, which was calculated to be the second excited state in C_5H_6. Due to the inability of CC2 to treat double excitations correctly,[64] the calculated

Table 1 Properties of the employed solvents at 20 °C. If not otherwise indicated, dipole moments were calculated by CC2/aug-cc-pVDZ

Solvent	Density/g cm^{-3}	Dipole moment/D	Viscosity/mPa s
Cyclohexane	0.78 (ref. 32)	0.00	0.98 (ref. 32)
Isopropanol	0.78 (ref. 33)	1.61	2.5 (ref. 33)
Chloroform	1.47 (ref. 34)	1.04 (ref. 35)	0.56 (ref. 34)
Trichloroethanol	1.56 (ref. 36)	2.04 (ref. 37)	21 (ref. 38)

energy might be inaccurate. However, as will be discussed later, the role of this state is not significant for the observed dynamics.

The 3A′ state has the character of a $n\pi^*$ excitation from the HOMO−2, which is a linear combination of two p-AOs of the chlorine atoms at the sp^3 hybridized carbon atom, to the LUMO. Thus, the state has no analogue in C_5H_6. Furthermore, it can be expected to play an important role in the photo-induced bond fission, since one of the chlorine atoms is directly involved in the reaction. Moreover, the p-AO of the remaining chlorine atom comes in resonance with the π-system of the five-membered ring in the course of planarization of the C_5Cl_5 radical (D_{5h} symmetry) after the bond fission.

As can be estimated from the spectra as well as the calculated excitation energies, bromination mainly leads to a considerable red shift of the absorption spectrum but not to a qualitative change in the excited state structure. Only the calculated states 2A′ and 3A′ interchange their character.

While different substituents at the carbon ring have considerable influence on the steady-state absorption spectra, the solvent plays a rather small role (for solvent properties see Table 1). Different solvents only lead to minor shifts in absorption maxima (for spectra in different solvents see Fig. S2 in the ESI†).

3.2 Transient absorption spectroscopy in solution

3.2.1 C_5Br_6. The photoinduced dynamics leading from photoexcitation into the 1A″ state to formation of CT complexes were investigated by transient absorption (TA) spectroscopy. In the TA traces of C_5Br_6 the observed features are only slightly solvent-dependent. In Fig. 2 the transients taken in cyclohexane
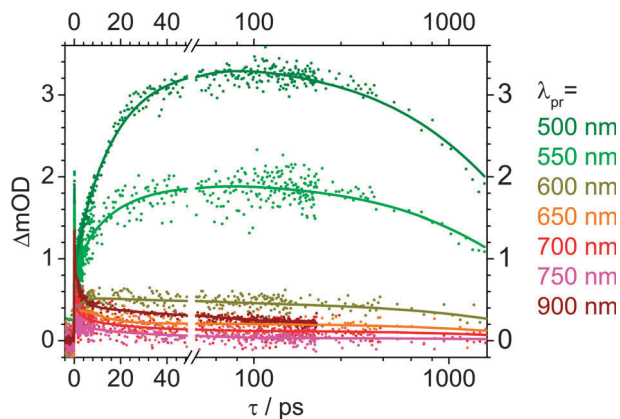

Fig. 2 Transient absorption traces (symbols) of C_5Br_6 in cyclohexane and global fit analysis (lines). Molecules are excited at λ_p = 350 nm.
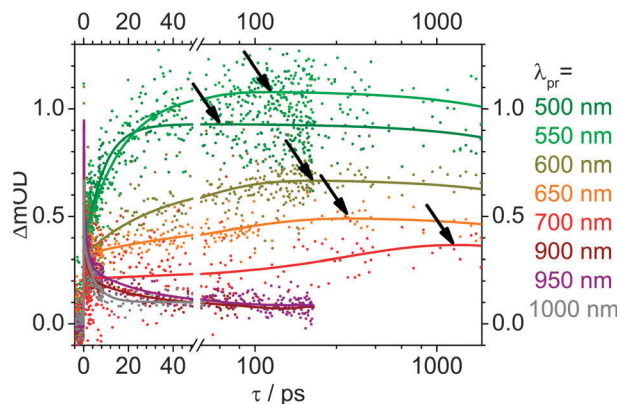
Fig. 3 Transient absorption traces (symbols) of C_5Br_6 in trichloroethanol and global fit analysis (lines). Molecules are excited at $\lambda_p = 350$ nm and probed at the λ_{pr} listed in the figure. The TA maximum shifts to longer delay times at longer λ_{pr} as indicated by the arrows. For transient spectra of C_5Br_6 in trichloroethanol constructed from the transient absorption traces, see Fig. S6 in the ESI.†

Fig. 4 Transient absorption traces (symbols) of C_5Cl_6 in isopropanol and global fit analysis (lines). Molecules are excited at $\lambda_p = 323$ nm. Inserted is a more detailed plot of the transient absorption evolution within the first ps.

are shown. The TA intensity initially prepared at time zero can be attributed to absorption of the excited 1A″ state and decays within <100 fs irrespective of the employed λ_{pr} or solvent. After the initial decay the evolution of TA is highly dependent on λ_{pr}: at short λ_{pr} (500–600 nm in the case of cyclohexane) the TA grows again within few tens of ps and decays on a time scale, which is beyond the experimentally accessible time window of 1.6 ns. At long λ_{pr} (650–900 nm for cyclohexane) the TA only decays to a value which is constant within the investigated time window. Obviously, in the spectral region between 500 and 600 nm the formation of a new absorption band can be observed. Its spectral signature fits well together with the earlier observed CT absorption bands of C_5Br_6.[18]

In trichloroethanol, isopropanol and chloroform (see Fig. 3, Fig. S3 and S4 in the ESI†) similar behavior is observed. However, the TA intensities at time zero and at the maxima of the forming absorption bands are lower and their spectral width is broadened in the chlorinated solvents. Thus, the solvent influence on the dynamics seems to be mostly of quantitative nature slightly influencing the transition strengths at the λ_{pr}. The samples of C_5Br_6 in isopropanol and trichloroethanol also show slight qualitative differences, a red-shift of the maximum of the CT band with time delay, which is marked by arrows in Fig. 3 and Fig. S3 in the ESI.† The appearance of the shift can be correlated with a higher polarity and viscosity of isopropanol and trichloroethanol in comparison to the other two solvents (see Table 1 for a list of solvent properties).
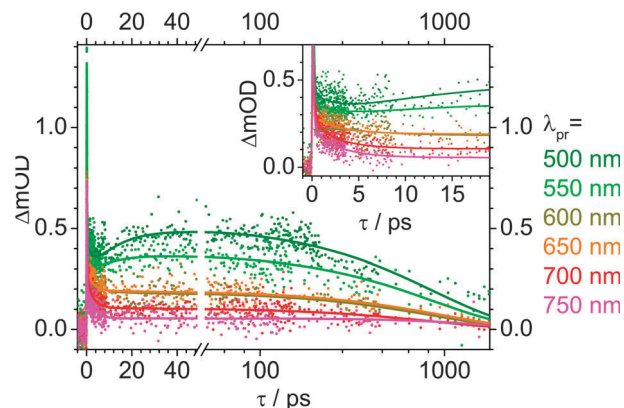
The experimental data are fitted with a 4-fold exponential function employing a Levenberg–Marquardt routine (see ESI,† Section 3 for details), where the time constants τ_1, τ_2 and τ_4 are adjusted globally for all TA traces in one specific solvent. τ_3 was also adjusted globally for the solvents cyclohexane and chloroform. However, in the case of isopropanol and trichloroethanol τ_3 had to be optimized for each λ_{pr} individually to model the observed spectral shift of the CT band maximum. The values of the time constants are listed in Table 2.

3.2.2 C_5Cl_6. In comparison to C_5Br_6 the TA traces of C_5Cl_6 in isopropanol, cyclohexane, trichloroethanol, and chloroform (see Fig. 4–6 and Fig. S5 in the ESI,† time constants are listed in Table 3) exhibit a more pronounced solvent dependence. The TA traces of C_5Cl_6 in isopropanol and chloroform (Fig. 4 and Fig. S5 in the ESI†) show behavior which is qualitatively similar to the observations in C_5Br_6. This is in contradiction to earlier studies, where no CT band in the visible was observed.[17] The major differences to the observations in C_5Br_6 are the time scales of rise and depletion of the TA at short λ_{pr}.

Furthermore, TA traces in trichloroethanol (Fig. 6) exhibit a rise of TA at short λ_{pr} on the ps timescale, but in the solvents isopropanol and chloroform the TA is quenched on the ps time scale. In this case a similar spectral shift of the transient TA maximum is found to that in the TA of C_5Br_6 in isopropanol and trichloroethanol.

In the TA traces of C_5Cl_6 in cyclohexane (Fig. 5) the initial TA intensity decays within <100 fs like in the other solvents (see the inset in Fig. 4). In sharp contrast to the other samples no rise of TA intensity at short λ_{pr} on the ps time scale is observed.

Table 2 Time constants and confidence intervals from global fit analyses (see Fig. S3, ESI) of C_5Br_6 TA traces in different solvents. Additionally, it is mentioned in the table whether the time constant is associated with a rise or decay of the TA. Time constants are optimized by a global fitting routine. Only in the case of isopropanol and trichloroethanol τ_3 is optimized separately for each λ_{pr}

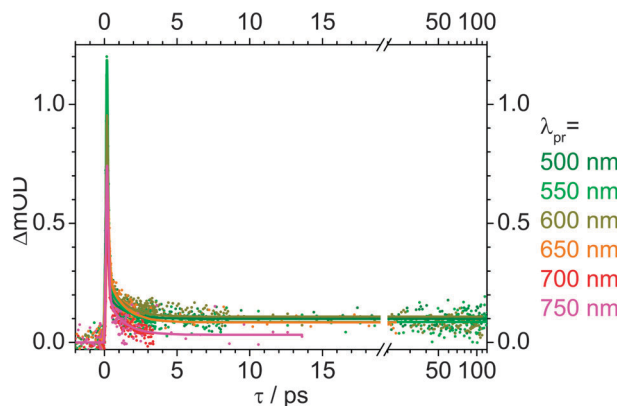| Solvent	τ_1/ps decay	τ_2/ps decay	τ_3 range/ps rise	τ_4/ps decay
Cyclohexane	0.07 ± 0.02	2.3 ± 0.4	17 ± 2	$>2 \times 10^3$
Isopropanol	0.07 ± 0.03	5 ± 1	$(27 \pm 1) - (110 \pm 30)$	$>2 \times 10^3$
Chloroform	0.05 ± 0.03	9 ± 3	28 ± 4	$>2 \times 10^3$
Trichloroethanol	0.07 ± 0.02	1.6 ± 0.4	$(8.0 \pm 0.8) - (400 \pm 100 \text{ fs})$	$>2 \times 10^3$

Fig. 5 Transient absorption traces (symbols) of C_5Cl_6 in cyclohexane and global fit analysis (lines). Molecules are excited at λ_p = 323 nm.
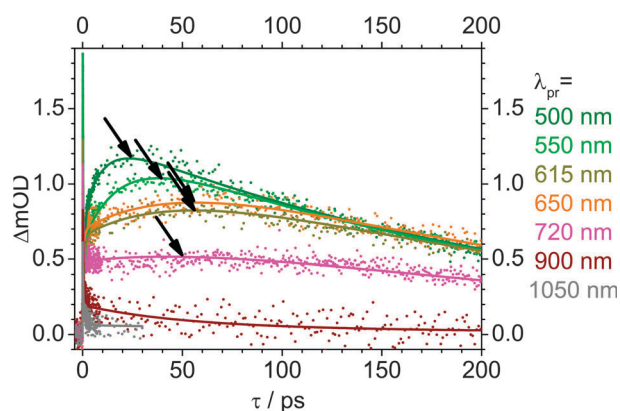

Fig. 6 Transient absorption traces (symbols) of C_5Cl_6 in trichloroethanol and global fit analysis (lines). Molecules are excited at λ_p = 323 nm. The TA maximum shifts to longer delay times at longer λ_{pr} as indicated by the arrows.

3.3 Time resolved photoelectron spectroscopy

To disentangle excited state dynamics from ground state dynamics and solute–solvent interaction, the photoinduced dynamics of C_5Cl_6 and C_5Br_6 were investigated in the gas phase by time resolved photoelectron spectroscopy (TRPES). TRPES spectra of C_5Cl_6 (λ_p = 315 nm, λ_{pr} = 267 nm and 400 nm) are shown in Fig. 7 (a) and (b). For details on the data processing and the fitting procedure see ESI,† Section 4. Two components can be distinguished in the TRPES spectrum at λ_{pr} = 267 nm resulting from a [1,2'] ionization: around time zero we observe a very short lived and spectrally broad photoelectron band ranging from 0 to 3.5 eV. A second band, which is spectrally narrower (0–1.3 eV), persists throughout the whole
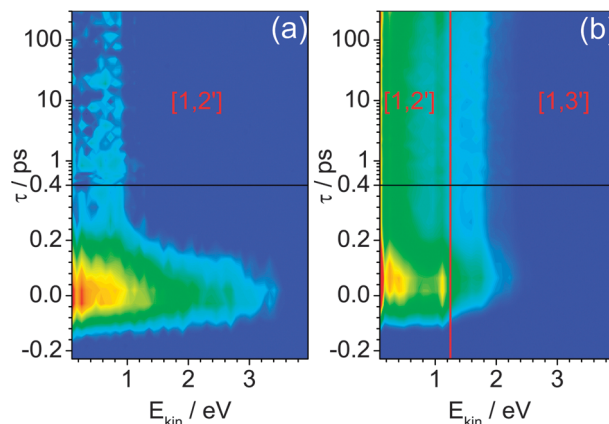

Fig. 7 Time resolved photoelectron spectra of C_5Cl_6 at λ_p = 315 nm and (a) λ_{pr} = 267 nm and (b) λ_{pr} = 400 nm. In the latter spectrum the cutoff between [1,2'] and [1,3'] photon ionization at 1.26 eV is inserted.

Table 4 Time constants and confidence intervals from global fit analyses of the TRPES spectra with doubly exponential decay functions (see ESI, Sections 4 and 5)

Sample	λ_{pr}/nm	τ_1/ps	τ_2/ps
C_5Cl_6	267	0.09 ± 0.01	>1 × 10³
C_5Cl_6	400	0.07 ± 0.01	>1 × 10³
C_5Br_6	400	0.15 ± 0.01	>1 × 10³

investigated time window of 300 ps. Both features are also found in the TRPES spectrum at λ_{pr} = 400 nm (see Fig. 7 (b)). However, the spectral narrowing between short lived and persisting bands is not as pronounced as at λ_{pr} = 267 nm. In comparison to the data at λ_{pr} = 267 nm the signature of the short lived band is more confined (0–3 eV) and the signature of the persisting band more broadened (0–2.5 eV). Furthermore, both photoelectron bands observed at λ_{pr} = 400 nm are more structured than the corresponding ones at λ_{pr} = 267 nm. The difference can be attributed to the energy cutoff between [1,2'] and [1,3'] photon ionization, which is also marked in the spectrum.

The spectra are fitted with two exponential functions. The resulting time constants are listed in Table 4. In both data sets a very short time constant τ_1 of 0.07–0.09 ps is found. It is connected to the discussed spectral change within the first 100 fs after time zero. τ_2 models the decay of the stable band and is therefore set to a high value, which cannot be specified in more detail by the available data.

Due to the small vapor pressure of C_5Br_6,[40] only TRPES spectra with a low count rate were recorded (see ESI,† Section 5).

Table 3 Time constants and confidence intervals from global fit analyses (see ESI, Section 3) of the C_5Cl_6 TA traces in different solvents. Additionally, it is mentioned in the table whether the time constant is associated with a rise or decay of the TA. Time constants are optimized by a global fitting routine. Only in the case of trichloroethanol τ_3 is optimized separately for each λ_{pr}

Solvent	τ_1/ps decay	τ_2/ps decay	τ_3 range/ps rise	τ_4/ps decay
Cyclohexane	0.07 ± 0.03	1.1 ± 0.3		>2 × 10³
Isopropanol	0.09 ± 0.01	2.9 ± 0.7	12 ± 2	900 ± 100
Chloroform	0.06 ± 0.02	2.1 ± 0.8	15 ± 2	>2 × 10³
Trichloroethanol	0.06 ± 0.01	1.7 ± 0.1	(12 ± 1) – (150 ± 30)	220 ± 2

This journal is © the Owner Societies 2013

Phys. Chem. Chem. Phys., 2013, **15**, 6673–6683 | **6677**

Nevertheless, they evinced the same features as do the spectra of C_5Cl_6. The time constants resulting from a fit with two exponential functions are listed in Table 4. In agreement with the findings for C_5Cl_6 a very short time constant $\tau_1 = 0.15$ ps and a time constant τ_2 with a value beyond the experimentally accessible time scale are found.

4 Discussion

4.1 Dynamics on the fs time scale

The gas phase dynamics of both C_5Cl_6 and C_5Br_6 shows only one single concerted reaction step associated with τ_1 and leads to a species, which is stable over the course of the experiment. From the knowledge of the photoinduced reactions in solution[17,18] we assign the step to homolytic fission of a carbon–halogen bond at the sp^3 position of the five-membered ring. The assignment is strongly supported by the absorption spectra of C_5Cl_5 and C_5Br_5 in solution, which exhibit – apart from temperature-dependent CT absorptions in the visible – further absorption bands at around 400 nm.[17,18] Moreover, the calculated absorption spectrum of C_5Cl_5 (see ESI,† Section 7) shows additional transitions with high oscillator strengths at around 267 nm. A resonant photoionization at both wavelengths can explain the high intensities of the stable photoelectron bands in the TRPES spectra.

Furthermore, a large fraction of the photoenergy from the pump pulse (C_5Cl_6: 3.84 eV, C_5Br_6: 3.54 eV) is converged to the dissociation reaction of C_5Cl_6 (typical C–X dissociation energies: 3.55 eV (Cl), 2.94 eV (Br)[65]) and the kinetic energy of the leaving chlorine atom. Hence, the photoproduct C_5Cl_5 can be expected to be only moderately vibrationally excited. This leads to a good Franck–Condon overlap between the C_5Cl_5 ground state and the lowest cationic state and, thereby, to an intense spectral signature as observed in the experimental data.[66]

In an alternative interpretation of the data one could assign the observed dynamics to relaxation into the ground state and the stable photoelectron band to ground state absorption of vibrationally "hot" molecules. This, however, is unlikely since such "hot" molecules would have a poor Franck–Condon overlap with the ionic manifold. Additionally, large amplitude motions of the carbon ring are expected to take place during the conversion into the ground state, which would lead e.g. to time-dependent spectral shifts in the photoelectron bands.[66] Since such an observation cannot be made in the TRPES spectra, we assign the stable feature of both C_5Cl_6 and C_5Br_6 to resonant ionization of C_5X_5 radicals. Accordingly, bond fission must be connected to τ_1 and takes place on the sub-100 fs time scale.

Another fact supporting the assignment is the observed early dynamics of C_5X_6 in solution. The initial decay of TA after time zero takes place on the same time scale as the signal decay in the TRPES spectra. Thus, the time constants τ_1 observed in gas phase and solution are likely to refer to the same processes. The dynamics following the initial decay can, therefore, be connected to processes involving the two radicals C_5X_5 and X. This kind of process is typically not observable in gas phase, since a solvent cage keeping the two radical species together is missing.

4.2 Experimental observation of the geminate CT complex generation

As already mentioned, the rise of the C_5Br_6 TA-signal at short λ_{pr} fits well together with the known CT absorption bands in a frozen solvent resulting from a geminate $[C_5Br_5\cdots Br]$ complex.[18] Compared to the spectral signature observed here the earlier reported CT absorption band is slightly blue-shifted with the maximum at 480 nm. The shift is most probably due to the difference in temperatures. The earlier observations were made at liquid nitrogen temperature, the present experiments at 20 °C.

CT complexes of bromine radicals with different solvents are known to exhibit absorption bands in the UV.[10] Hence, the absorption bands observed here cannot originate from interaction between the bromine radical and the solvent and have to be assigned to a geminate CT complex of the two radicals. Furthermore, in earlier experiments melting of the solvent led to disappearance of the absorption bands,[18] which has to be due to dissociation of the CT complex. Other mechanisms like recombination and an electron transfer reaction cannot account for the disappearance, since the first takes place on shorter time scales[14,67,68] and the latter is not favored as already discussed in the Introduction. Thus, the CT band intensity is a good tool for investigating the formation and dissociation of the geminate CT complex.

As opposed to C_5Br_6, geminate CT absorption bands in the visible originating from photolyzed C_5Cl_6 were not observed earlier.[17,18] The solvent, which was employed at that time, was 3-methylpentane, an apolar hydrocarbon like the solvent cyclohexane. Therefore, these findings are in agreement with the present observations, since C_5Cl_6 does not exhibit a transient absorption band in the visible when dissolved in cyclohexane. Furthermore, CT complexes of Cl radicals with the solvent exhibit absorptions in the UV.[7,11] Thus, the TA rise on the ps time scale can also be absorption of a geminate CT complex.

4.3 Theoretical investigation of generation and character of CT complexes

Possible structures of the photolyzed C_5X_6 were investigated by BP86/def2-SV(P). Due to disproportionately computational demand no solvent could be included into the calculations. Only one minimum with C_s symmetry could be found, where the leaving halogen atom is loosely bound to another halogen ring substituent. The halogen–halogen bond is thereby directed perpendicularly to the planar C_5X_5 ring system (see Fig. 8 (a)). The distance between the Cl (Br) atoms is 250 pm (270 pm), which is considerably larger than the bond distance of Cl_2 (Br_2) (199 pm (229 pm)).[65] The dissociation energy of the complex is estimated to be 28 (33) kJ mol^{-1} (for details see Section 6 in the ESI†). Additionally, TDDFT calculations reveal that these species also exhibit a very strong transition in a suitable spectral region to account for the experimentally observed absorption band (see Fig. 9). According to a Mulliken population analysis in the ground state, the loosely bound Cl (Br) exhibits a slightly negative charge of -0.34 (-0.25) and the nearest Cl (Br) ring substituent a positive charge of 0.21 (0.60). Thus, it is most

6678 | Phys. Chem. Chem. Phys., 2013, 15, 6673–6683

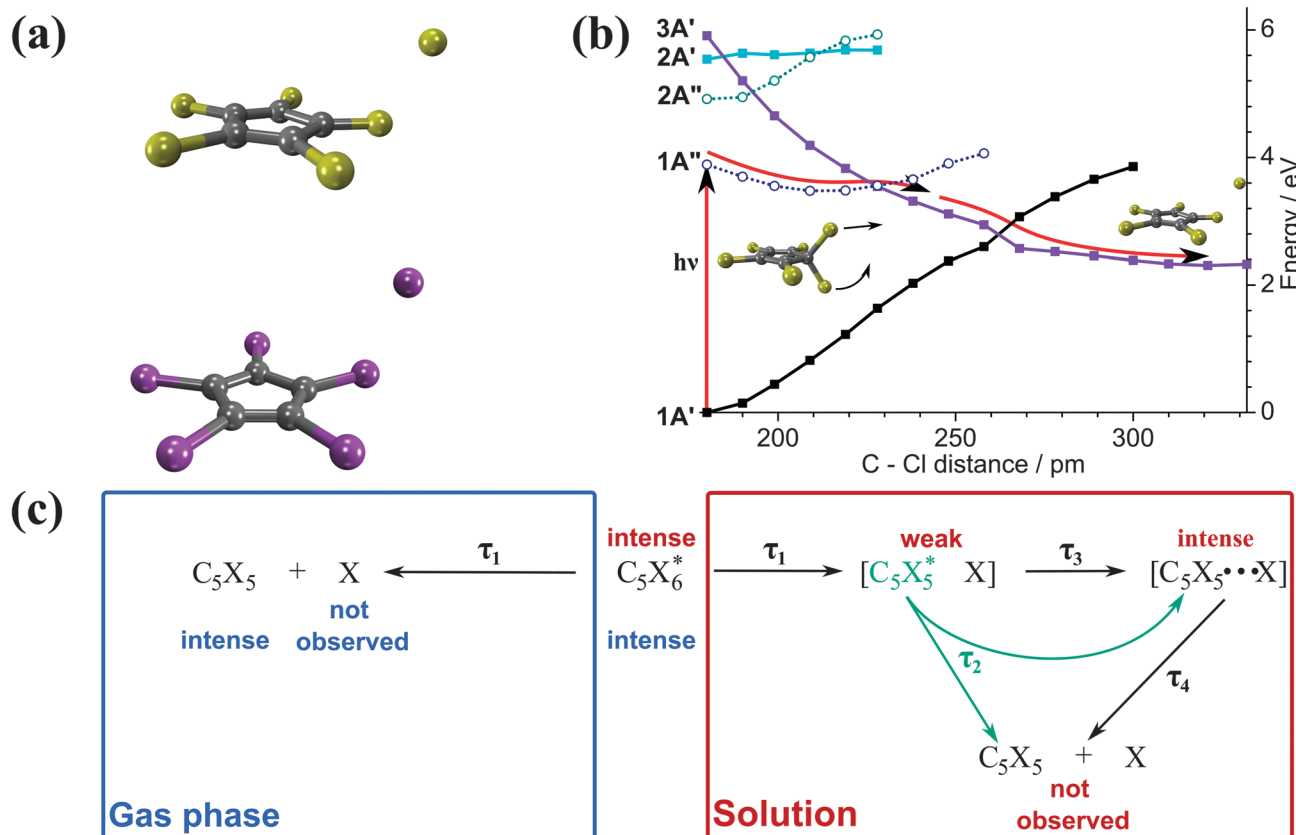This journal is © the Owner Societies 2013

Fig. 8   (a) CT complex structures of $C_5Cl_5\cdots Cl$ (above) and $C_5Br_5\cdots Br$ (below) optimized by BP86/def2-SV(P). (b) Interpolated path between the minimum of C_5Cl_6 and the optimized CT complex minimum calculated at the CC2/aug-cc-pVDZ level of theory. The abscissa resembles the C–Cl bond dissociation coordinate. The states with A′ symmetry including the ground state are labeled by solid lines, the states with A″ symmetry by dotted lines. The proposed relaxation pattern is marked by arrows. It includes the 1A′ ground state (black), the 1A″ state (dark blue), which the molecule is excited into, and the 3A′ state (violet). Intervening states 2A″ (green) and 2A′ (light blue) are shown not to play a significant role. (c) Relaxation scheme for C_5Cl_6 and C_5Br_6 in the gas phase (blue) and in solution (red). The intensities of the generated species in the experimental data are additionally mentioned. After photoexcitation $C_5X_6^*$ directly dissociates in the gas phase with a time constant τ_1. In solution the same process is also found, but leads to formation of a geminate radical pair $[C_5X_5^* \; X]$ in a joint solvent cage. Formation of the CT complex $[C_5X_5\cdots X]$ associated with τ_3 is accompanied by vibrational cooling of the $C_5X_5^*$ radical fragment (green) associated with τ_2. The CT complex formation competes with escape of the halogen radical from the joint solvent cage, which cannot be directly observed in the experimental data. Quenching of the CT complex is connected to τ_4.

probable that within the transition the CT takes place from the loosely bound halogen to the five-membered ring system.

An interpolated path between the C_5Cl_6 minimum and the minimum of the optimized species (see Fig. 8 (b)) at the CC2/aug-cc-pVDZ level of theory reveals a possible relaxation path in the direction of the $C_5Cl_5\cdots Cl$ species. The abscissa resembles the C–Cl bond dissociation coordinate. The states with A′ symmetry are labeled by solid lines, the states with A″ symmetry by dotted lines. The discussion of the interpolated path can be reduced to the ground state of C_5Cl_6 and the excited states, which are marked in Fig. 1 (a): photoexcitation from the ground state (black) promotes the molecule to the first excited state with A″-symmetry (blue). Planarization of the C_5Cl_5 ring and detachment of the Cl atom lead to a moderate lowering of the 1A″ state and a substantial lowering of the 3A′ state resulting in a crossing. This state seems to be the ground state at the optimized $C_5Cl_5\cdots Cl$ minimum. Thus, the speculations from Section 3.1 about the role of the 3A′ state are strongly supported. Planarization of C_5Cl_5 and departure of the Cl atom lead to energy lowering of the LUMO due to

interaction with the p-AO of the planarized Cl atom and to a rise of the energy of the HOMO−2 (see Fig. 1 (a)). An influence of the state, which is the ground state at the C_{2v} minimum, as it is suggested by the projection of the interpolated path, is possible, but not definitive. Furthermore, the 2A′ state can be neglected in the interpolation. An analogous interpolation was also done for C_5Br_6. The results are qualitatively comparable (see Fig. S12 in the ESI†).

Since CC2 is known to poorly treat excited states with doubly excited character[64] and the second excited state of C_5H_6 is known to have a multiconfigurational character with considerable contribution of a LUMO ← HOMO double excitation, the CC2 results are re-evaluated by recalculating the same interpolated path for C_5Cl_6 employing SA-4-CASSCF(6,5)/6-31G*[60–63] (see Fig. S11 and a description of the employed CAS in the ESI†). Although the results are not quantitative, CASSCF is able to treat multiconfigurational states with doubly excited character qualitatively correctly. The results are in agreement with the CC2 results. An excited state comparable to the one in C_5H_6 is found, but it does not interfere with the three states

considered above. As already discussed, the 3A′ state has no analogue in C_5H_6. Therefore, the analogous CT complex structure cannot be optimized and this reaction channel is absent in C_5H_6.

4.4 Mechanism of CT complex generation

Despite the highly simplified picture presented by the interpolated path, it allows for an explanation of the experimentally observed excited state dynamics which we summarize in the reaction scheme in Fig. 8 (c): upon relaxation in the 1A″ state, photoexcited C_5X_6 reaches a surface crossing between 1A″ and 3A′ leading to population transfer to 3A′, which is associated with the time constant τ_1. In the gas phase (left part of Fig. 8 (c)) leaving of the halogen atom is not hindered and the two radicals separate ballistically.

In solution (right part of Fig. 8 (c)) geminate radicals are generated in a joint solvent cage ($[C_5X_5^*\ X]$) by the bond dissociation. Their spectral signatures are presumably governed by the absorption of the vibrationally excited $C_5X_5^*$ radical (colored in green in Fig. 8 (c)). Its lowest absorption band peaks at around 400 nm[17,18] outside of the investigated spectral window. Thus, the observed weak TA after the bond dissociation probably originates from the red-shifted absorption band of $C_5X_5^*$ due to the vibrational excitation.

This is best observable in the case of C_5Cl_6 in cyclohexane, where the subsequent formation of a CT absorption band is missing. Accordingly, the chlorine radical is in this case able to escape from the joint solvent cage before the $[C_5Cl_5\cdots Cl]$ complex can be formed, since photoinduced generation of C_5Cl_5 radicals was observed earlier by EPR spectroscopy in apolar solvents.[17] Cage escape processes are known to take place on compatible time scales.[14,67,68] Thus the decay of the weak signature connected to τ_2 is most likely connected to vibrational cooling of $C_5Cl_5^*$. However, a contribution of geminate recombination of the radicals cannot be fully excluded, since it typically takes place on an analogous time scale.[12] However, if recombination takes place, it is definitely in competition with an escape of the halogen radical.

In the other samples the separation of the halogen radical from the C_5X_5 radical can be at least partially prevented by solvent caging. Thus, relaxation of the geminate radicals $[C_5X_5^*\ X]$ into the CT complex minimum $[C_5X_5\cdots X]$ is possible. This relaxation is connected to a considerable growth in TA intensity in the blue part of the investigated spectral window, since it leads to formation of the CT absorption band. Accordingly, the process can be associated with τ_3, which is represented by the TA growth in the fits.

Furthermore, in all samples and irrespective of the solvent, time constants τ_2 with comparable spectral signatures and values were found (compare *e.g.* the inset in Fig. 4 with Fig. 5) and were assigned to the vibrational cooling of the $C_5X_5^*$ fragment. However, it cannot be determined by the experimental data alone whether this indicates a competition between escape of the halogen atom from the solvent cage and formation of CT complexes in all investigated solvents.
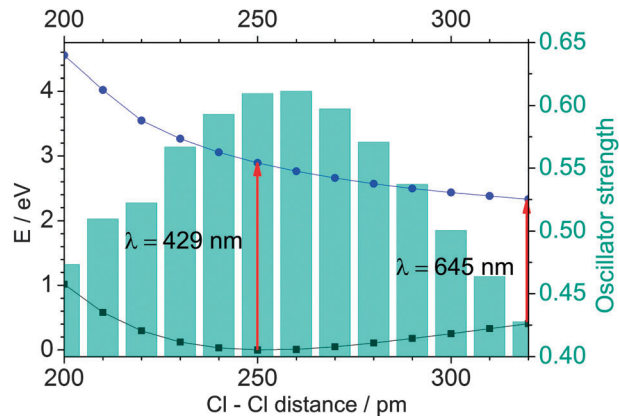

Fig. 9 Results from a coordinate scan of the $C_5Cl_5\cdots Cl$ CT-complex dissociation by TDDFT/aug-cc-pVDZ. The dissociation coordinate is chosen to be the distance between the loosely bound chlorine atom and its nearest neighbor, a chlorine ring substituent. The black dots represent ground state energies of the CT complex, the blue dots represent energies of the lowest excited state with considerable oscillator strength. Additionally, the calculated oscillator strength of the transition between the two states dependent on the dissociation coordinate is depicted as bars. Enlargement of the bond distance leads to a considerable red-shift and weakening of the calculated CT absorption band.

The observed CT complexes disappear on the time scale of τ_4 (see Fig. 8 (c)). The nature of the underlying quenching process and the reasons for the highly solvent-dependent lifetimes are discussed in the following.

4.5 Spectral shift of the CT absorption band

The geminate CT absorption band can be expected to be sensitive even to small changes in the distance between the radicals. Therefore, we propose that the observed spectral shifts in the CT absorption band (see Fig. 3 and 6, and Fig. S3 in the ESI†) are an indicator for a change in this distance. To support this interpretation, the dissociation coordinate of the $C_5Cl_5\cdots Cl$ complex, *i.e.* the "bond" length between the Cl radical and the nearest Cl ring substituent, is scanned by TDDFT/B3LYP/aug-cc-pVDZ. TDDFT is not ideally suitable to describe excitation energies to CT states,[69–71] but this flaw can partly be compensated by the use of hybrid functionals like B3LYP, as employed in the present case.[72] In Fig. 9 the energies of the ground state and the excited state with the by far strongest oscillator strength are depicted as a function of the Cl–Cl separation. Furthermore, the oscillator strengths for the transition at all calculated distances are shown as bars. Although the transition energies are slightly overestimated by the calculation, the plot gives a qualitative explanation for the observed spectral shift of the CT absorption band. Upon increasing the Cl–Cl distance, the transition resonance shifts towards longer wavelengths and, simultaneously, the band intensity weakens. Thus, on the time scale of the spectral shift, motion of the halogen radical away from the cyclopentadienyl radical is observable.

4.6 The fate of the CT complex

The next question one might ask would be whether the motion of the halogen radical can also account for the quenching

mechanism of the CT complex. In most cases, this can be ruled out by a comparison of the range of τ_3 values with the observed τ_4 values (see Tables 2 and 3). They differ by at least one order of magnitude. The only exception is C_5Cl_6 in trichloroethanol, where the values are comparable. This will be discussed in detail below.

A second issue to address is, if one of the two processes, spectral shift and CT complex quenching, exhibits a diffusive character. This can be decided by comparing their time scales to the time scale of diffusional motion. The time scale of the spectral shift can be quantified by the range of τ_3 in Tables 2 and 3. The time-dependence of the distance expectation value in diffusion is:[73]

$$\langle d^2 \rangle = 2Dt \qquad (1)$$

By employing the Stokes–Einstein relation for the diffusion coefficient D of a single radical species

$$D = \frac{k_B T}{6\pi\eta r}, \qquad (2)$$

one can evaluate the time, which is needed by the two radicals to diffuse an average distance $\sqrt{\langle d^2 \rangle}$ by

$$t = \frac{\langle d^2 \rangle 6\pi\eta r_A r_B}{2k_B T (r_A + r_B)}. \qquad (3)$$

The distance of diffusion is chosen to be the calculated equilibrium distance in the CT complex, i.e. an estimation is made about the time it takes for the radicals to achieve twice the bond distance (250 pm ($C_5Cl_5\cdots Cl$) vs. 270 pm ($C_5Br_5\cdots Br$)). The radii of the radicals are estimated to be $r_A = 522$ pm (C_5Cl_5) and 560 pm (C_5Br_5). r_B is estimated to be 100 pm (Cl) and 115 pm (Br), which are the covalent radii of the elements.[65] Solvent viscosities are taken from Table 1. Chloroform exhibits the lowest viscosity ($\eta = 0.56$ mPa s) and trichloroethanol the highest ($\eta = 21$ mPa s).

The time values calculated for $C_5Cl_5\cdots Cl$ range between 7 and 260 ps and between 11 and 410 ps for $C_5Br_5\cdots Br$, depending on the solvent viscosity, which is in reasonably good agreement with the range of τ_3 values found in connection to the spectral shift. The shift could, therefore, be caused by a diffusional process. Comparison with the time scale of the CT band decay (τ_4) however shows a difference by an order of magnitude in most cases. A diffusive character of the quenching mechanism can, therefore, be excluded. It can be speculated that within the minimum of the CT complex diffusion is possible to a small extent, which then accounts for the observed spectral shift.

The comparison gives an additional hint for the nature of the CT complex. Apparently, its stabilization is not of purely sterical nature due to the solvent cage. As other groups found comparable time scales of CT absorption quenching in similar systems,[14] the present case does not seem to be exceptional. As opposed to earlier investigations, the lifetime of the CT absorption is not due to a halogen radical forming transient CT species with solvent molecules during diffusion, but due to a considerably stronger interaction between two individual species.

The quenching, therefore, must be either due to a thermal cleavage reaction or due to direct reaction of the radicals constituting the CT complex with molecules from the solvent cage. It can only be speculated about the reactivity of the C_5X_5 radical. The most probable reaction is reduction to the anion, which is a stable aromatic. Due to a lower steric demand, however, the reactivity of the halogen radicals can be expected to have a higher influence on the quenching of the CT complex. Cl radicals are known to form CT complexes with halogenated solvents exhibiting absorption bands in the UV.[7,11] Unlike Br radicals, which are known to be rather unreactive in solution and have lifetimes in the μs range in many solvents,[5,6,8–10,14] they undergo rapid reaction with solvent molecules under H abstraction.[12,13,74] These reactions are assumed to be very fast in the case of aliphatic hydrocarbons and alcohols. For example, the time constant for the reaction between Cl and cyclohexane was measured to be 20 ps.[74] Thus, the $C_5Cl_5\cdots Cl$ CT complex can be quenched by direct reaction of Cl radicals with molecules from the solvent cage. However, in the case of C_5Cl_6 in cyclohexane the formation of a charge transfer complex is not observed, which prevents the reaction from being investigated at least in the visible spectral range. Hydrogen abstraction from isopropanol was observed to take place with a time constant of 12 ps.[13] Comparison with the findings regarding the TA decay in isopropanol leads to the conclusion that direct reaction with the solvent cage cannot account for the TA quenching. The same also holds for chloroform. Thus, a thermal decomposition of the CT complex has to be assumed. Reactions of the halogen radicals following the decomposition do not seem to be observable in most solvents.

C_5Cl_6 in trichloroethanol, however, exhibits a TA decay, which is considerably faster than in the other solvents ($\tau_4 = 220$ ps). The finding is in good agreement with the estimated diffusion time of 260 ps. Additionally, the spectral shift, which can be connected to a motion of the radicals away from each other, is on a similar time scale. Therefore, such a motion, which is only controlled by diffusion and eventually leads to quenching of the CT complex, can be assumed.

The question remains, why a diffusional quenching process is only possible in trichloroethanol. It seems rather improbable that the CT complex is destabilized to such great amount by bulk solvent properties, since the properties of isopropanol are generally similar (see Table 1). A possible reason for the behavior is a removal of the barrier by a direct hydrogen abstraction channel involving a molecule from the solvent cage. H abstraction could be facilitated for trichloroethanol in comparison to isopropanol by the electron withdrawing effect of the chlorine substitution.

4.7 Conclusion

The two systems C_5Cl_6 and C_5Br_6 have been investigated by femtosecond time-resolved pump–probe spectroscopy in the gas phase and various solvents. Upon irradiation they perform homolytic bond dissociation both in the gas phase and in solution within $\tau_1 < 100$ fs. Following the bond dissociation in solution, geminate formation of a CT complex is observed on

the time scale of several ps. It thereby competes with escape of the halogen radical from the solvent cage and geminate recombination of the radicals taking place within few ps. The competition is thereby highly solvent dependent in the case of C_5Cl_6. The CT complexes are observed to be surprisingly stable in most solvents. In the solvent trichloroethanol the $C_5Cl_5\cdots Cl$ CT complex is observed to be less stable by an order of magnitude than in the other solvents, which can be regarded as a hint for a direct H abstraction reaction of the Cl radical with a molecule from the solvent cage.

Acknowledgements

References

1 D. Vione, V. Maurino, C. Minero, E. Pelizzetti, M. A. J. Harrison, R.-I. Olariu and C. Arsene, *Chem. Soc. Rev.*, 2006, **35**, 441–453.

2 M. A. Tasdelen and Y. Yagci, *Aust. J. Chem.*, 2011, **64**, 982–991.

3 B. Halliwell, *Mutat. Res., Genet. Toxicol. Environ. Mutagen.*, 1999, **443**, 37.

4 S. Rayne, K. Forest and K. J. Friesen, *Environ. Int.*, 2009, **35**, 425–437.

5 N. Yamamoto, T. Kajikawa, H. Sato and H. Tsubomura, *J. Am. Chem. Soc.*, 1969, **91**, 265–267.

6 J. M. Bossy, R. E. Buehler and M. Ebert, *J. Am. Chem. Soc.*, 1970, **92**, 1099–1101.

7 J. E. Chateauneuf, *Chem. Phys. Lett.*, 1989, **164**, 577–580.

8 L. C. T. Shoute and P. Neta, *J. Phys. Chem.*, 1990, **94**, 2447–2453.

9 L. C. T. Shoute and P. Neta, *J. Phys. Chem.*, 1990, **94**, 7181–7184.

10 Z. B. Alfassi, R. E. Huie, J. P. Mittal, P. Neta and L. C. T. Shoute, *J. Phys. Chem.*, 1993, **97**, 9120–9123.

11 J. E. Chateauneuf, *J. Org. Chem.*, 1999, **64**, 1054–1055.

12 C. G. Elles, M. J. Cox, G. L. Barnes and F. F. Crim, *J. Phys. Chem. A*, 2004, **108**, 10973–10979.

13 L. Sheps, A. C. Crowther, C. G. Elles and F. F. Crim, *J. Phys. Chem. A*, 2005, **109**, 4296–4302.

14 S. L. Carrier, T. J. Preston, M. Dutta, A. C. Crowther and F. F. Crim, *J. Phys. Chem. A*, 2010, **114**, 1548–1555.

15 B. P. Fingerhut, C. F. Sailer, J. Ammer, E. Riedle and R. de Vivie-Riedle, *J. Phys. Chem. A*, 2012, **116**, 11064–11074.

16 J. Ammer, C. F. Sailer, E. Riedle and H. Mayr, *J. Am. Chem. Soc.*, 2012, **134**, 11481–11494.

17 F. Graf and H. H. Günthard, *Chem. Phys. Lett.*, 1970, **7**, 25–28.

18 F. Graf and H. H. Günthard, *Chem. Phys. Lett.*, 1971, **8**, 395–398.

19 P. Bachmann, F. Graf and H. Günthard, *Chem. Phys.*, 1975, **9**, 41–56.

20 W. Fuß, W. E. Schmid and S. Trushin, *Chem. Phys.*, 2005, **316**, 225–234.

21 T. Kovar and H. Lischka, *J. Mol. Struct.*, 1994, **303**, 71–82.

22 F. Rudakov and P. M. Weber, *Chem. Phys. Lett.*, 2009, **470**, 187–190.

23 O. Schalk, A. E. Boguslavskiy and A. Stolow, *J. Phys. Chem. A*, 2010, **114**, 4058–4064.

24 F. Rudakov and P. M. Weber, *J. Phys. Chem. A*, 2010, **114**, 4501–4506.

25 M. Z. Zgierski and F. Zerbetto, *Chem. Phys. Lett.*, 1991, **179**, 131–136.

26 L. Serrano-Andres, M. Merchan, I. Nebot-Gil, B. O. Roos and M. Fulscher, *J. Am. Chem. Soc.*, 1993, **115**, 6184–6197.

27 M. Z. Zgierski and F. Zerbetto, *J. Chem. Phys.*, 1993, **99**, 3721–3729.

28 H. Nakano, T. Tsuneda, T. Hashimoto and K. Hirao, *J. Chem. Phys.*, 1996, **104**, 2312–2320.

29 J. Wan, M. Ehara, M. Hada and H. Nakatsuji, *J. Chem. Phys.*, 2000, **113**, 5245–5252.

30 T. S. Kuhlman, W. J. Glover, T. Mori, K. B. Møller and T. Martinez, *Faraday Discuss.*, 2012, **157**, 193–212.

31 O. Schalk and A.-N. Unterreiner, *J. Phys. Chem. A*, 2007, **111**, 3231–3240.

32 Safety data sheet of cyclohexane, downloaded from Carl Roth 2012.07.18.

33 Safety data sheet of isopropanol, downloaded from Carl Roth 2012.07.18.

34 Safety data sheet of chloroform, downloaded from Carl Roth 2012.07.18.

35 E. S. Snow, F. K. Perkins, E. J. Houser, S. C. Badescu and T. L. Reinecke, *Science*, 2005, **307**, 1942–1945.

36 Safety data sheet of trichloroethanol, downloaded from Sigma Aldrich 2012.07.18.

37 S. S. Krishnamurthy and S. Soundararajan, *J. Phys. Chem.*, 1969, **73**, 4036–4039.

38 N. S. Angerman and R. B. Jordan, *J. Chem. Phys.*, 1971, **54**, 837–843.

39 http://www.analytical standards.com.

40 F. Strauss, L. Kollek and W. Heyn, *Ber. Dtsch. Chem. Ges. B*, 1930, **63**, 1868–1885.

41 T. J. A. Wolf, D. Voll, C. Barner-Kowollik and A.-N. Unterreiner, *Macromolecules*, 2012, **45**, 2257–2266.

42 E. Riedle, M. Beutter, S. Lochbrunner, J. Piel, S. Schenkl, S. Spörlein and W. Zinth, *Appl. Phys. B: Lasers Opt.*, 2000, **71**, 457–465.

43 I. Z. Kozma, P. Baum, S. Lochbrunner and E. Riedle, *Opt. Express*, 2003, **11**, 3110–3115.

44 S. Lochbrunner, J. J. Larsen, J. P. Shaffer, M. Schmitt, T. Schultz, J. G. Underwood and A. Stolow, *J. Electron Spectrosc. Relat. Phenom.*, 2000, **112**, 183–198.

6682 | *Phys. Chem. Chem. Phys.*, 2013, **15**, 6673–6683

This journal is © the Owner Societies 2013

45 G. K. Jarvis, M. Evans, C. Y. Ng and K. Mitsuke, *J. Chem. Phys.*, 1999, **111**, 3058–3069.

46 R. Ahlrichs, M. Bär, M. Häser, H. Horn and C. Kölmel, *Chem. Phys. Lett.*, 1989, **162**, 165–169.

47 O. Treutler and R. Ahlrichs, *J. Chem. Phys.*, 1995, **102**, 346–354.

48 K. Eichkorn, O. Treutler, H. Öhm, M. Häser and R. Ahlrichs, *Chem. Phys. Lett.*, 1995, **240**, 283–290.

49 K. Eichkorn, O. Treutler, H. Öhm, M. Häser and R. Ahlrichs, *Chem. Phys. Lett.*, 1995, **242**, 652–660.

50 F. Weigend, *Phys. Chem. Chem. Phys.*, 2006, **8**, 1057–1065.

51 A. Schäfer, H. Horn and R. Ahlrichs, *J. Chem. Phys.*, 1992, **97**, 2571–2577.

52 C. Hättig and F. Weigend, *J. Chem. Phys.*, 2000, **113**, 5154–5161.

53 C. Hättig and A. Köhn, *J. Chem. Phys.*, 2002, **117**, 6939–6951.

54 A. Köhn and C. Hättig, *J. Chem. Phys.*, 2003, **119**, 5021–5036.

55 R. A. Kendall, T. H. Dunning and R. J. Harrison, *J. Chem. Phys.*, 1992, **96**, 6796–6806.

56 F. Furche and D. Rappoport, *Computational and Theoretical Chemistry*, Elsevier, Amsterdam, 2005, vol. 16.

57 R. Bauernschmitt and R. Ahlrichs, *Chem. Phys. Lett.*, 1996, **256**, 454–464.

58 R. Bauernschmitt and R. Ahlrichs, *J. Chem. Phys.*, 1996, **104**, 9047–9052.

59 F. Weigend and R. Ahlrichs, *Phys. Chem. Chem. Phys.*, 2005, **7**, 3297–3305.

60 H. Lischka, R. Shepard, F. B. Brown and I. Shavitt, *Int. J. Quantum Chem.*, 1981, **20**, 91–100.

61 R. Shepard, I. Shavitt, R. M. Pitzer, D. C. Comeau, M. Pepper, H. Lischka, P. G. Szalay, R. Ahlrichs, F. B. Brown and J.-G. Zhao, *Int. J. Quantum Chem.*, 1988, **34**, 149–165.

62 H. Lischka, R. Shepard, R. M. Pitzer, I. Shavitt, M. Dallos, T. Muller, P. G. Szalay, M. Seth, G. S. Kedziora, S. Yabushita and Z. Zhang, *Phys. Chem. Chem. Phys.*, 2001, **3**, 664–673.

63 H. Lischka, T. Müller, P. G. Szalay, I. Shavitt, R. M. Pitzer and R. Shepard, *WIREs Comput. Mol. Sci.*, 2011, **1**, 191–199.

64 M. Schreiber, M. R. Silva-Junior, S. P. A. Sauer and W. Thiel, *J. Chem. Phys.*, 2008, **128**, 134110–134125.

65 CRC Handbook of Chemistry and Physics, ed. W. M. Haynes, CRC Press, Boca Raton, FL, 92nd edn, 2011–2012.

66 O. Schalk, A. E. Boguslavskiy, A. Stolow and M. S. Schuurman, *J. Am. Chem. Soc.*, 2011, **133**, 16451–16458.

67 I. Benjamin, *J. Chem. Phys.*, 1995, **103**, 2459–2471.

68 I. Chorny, J. Vieceli and I. Benjamin, *J. Chem. Phys.*, 2002, **116**, 8930–8937.

69 M. E. Casida, F. Gutierrez, J. Guan, F.-X. Gadea, D. Salahub and J.-P. Daudey, *J. Chem. Phys.*, 2000, **113**, 7062–7071.

70 A. Dreuw, J. L. Weisman and M. Head-Gordon, *J. Chem. Phys.*, 2003, **119**, 2943–2946.

71 K. Sadeghian and M. Schütz, *J. Am. Chem. Soc.*, 2007, **129**, 4068–4074.

72 D. Rappoport and F. Furche, *J. Am. Chem. Soc.*, 2004, **126**, 1277–1284.

73 H. J. V. Tyrrell and K. R. Harris, *Diffusion in liquids*, Butterworths, London, 1984.

74 D. Raftery, M. Iannone, C. Phillips and R. Hochstrasser, *Chem. Phys. Lett.*, 1993, **201**, 513–520.